Non-Abelian geometric phases in a system of coupled quantum bits

Vahid Azimi Mousolou*
Department of Physics and Electrical Engineering, Linnaeus University, 391 82 Kalmar, Sweden

Erik Sjöqvist†
Department of Quantum Chemistry, Uppsala University, Box 518, Se-751 20 Uppsala, Sweden
and Centre for Quantum Technologies, National University of Singapore, 3 Science Drive 2, 117543 Singapore, Singapore

(Received 28 November 2013; published 20 February 2014)

A common strategy to measure the Abelian geometric phase for a qubit is to let it evolve along an orange-slice-shaped path connecting two antipodal points on the Bloch sphere by two different semi-great-circles. Since the dynamical phases vanish for such paths, this allows for direct measurement of the geometric phase. Here, we generalize the "orange-slice" setting to the non-Abelian case. The proposed method to measure the non-Abelian geometric phase can be implemented in a cyclic chain of four qubits with controllable interactions.

DOI: 10.1103/PhysRevA.89.022117 PACS number(s): 03.65.Vf, 03.67.Lx

I. INTRODUCTION

The geometric phase (GP), first discovered by Berry [1] for adiabatic cyclic changes of pure quantum states, has been generalized to a wide range of contexts, such as nonadiabatic [2], noncyclic [3], non-Abelian [4,5], and mixed state [6,7] evolution. This purely geometric object is manifested in various theoretical and experimental areas, such as in optics, condensed matter physics, and molecular physics, as well as in quantum field theory, and more recently in quantum computation [8,9].

An essential ingredient when measuring the GP is to find techniques to remove the effect of dynamical phases associated with the Hamiltonian of the system. One such method is based on the fact that there are certain paths along which the dynamical phase vanishes. For two-level systems (qubits), the orange-slice-shaped path, formed by connecting two antipodal points on the Bloch sphere along two different semi-great-circles, is associated with vanishing dynamical phase, which allows for direct measurement of the GP. The orange-slice-shaped path has indeed been a common method to measuring the Abelian GP [10–14].

Here, we generalize the concept of the orange-slice-shaped path to the non-Abelian GP in nonadiabatic evolution [5]. The generalization can be realized by combining a pair of pulsed interactions in a cyclic chain of four coupled qubits. The resulting non-Abelian GP can be used for universal nonadiabatic holonomic single-qubit gates. Such gates have recently been proposed in Ref. [15] and experimentally realized in Refs. [16,17]. The interactions are assumed to be controllable and of combined XY and Dzyaloshinski-Moriya type. Typical physical systems for implementing the non-Abelian orange-slice-shaped path and corresponding GP could be coupled quantum dots [18], atoms trapped in an optical lattice [19], and surface states of topological insulators [20].

The outline of the paper is as follows. In the next section we review the basic idea of the orange-slice-shaped path for nonadiabatic evolution of a single qubit. We demonstrate how such a path can be implemented by applying an appropriate pair of pulses and how the resulting GPs can be used to realize a single-qubit phase-shift gate. In Sec. III, we generalize the orange-slice setting to the non-Abelian case. Here, the orange-slice-shaped path consists of pairs of geodesic segments in the Grassmann manifold describing the system. We further demonstrate how the resulting non-Abelian GP can be measured. The paper ends with the conclusions.

II. ABELIAN SETTING

We first describe the realization of the orange-slice-shaped path in the Abelian case of a single qubit. Let σ_x, σ_y, and σ_z be the standard Pauli operators and consider the Hamiltonian

$$H^{(\mathrm{a})}(t) = \tfrac{1}{2} f(t)[\cos(\phi)\sigma_x + \sin(\phi)\sigma_y], \tag{1}$$

where $f(t)$ and ϕ are externally controllable parameters; $f(t)$ defines the "pulse area" $\alpha_t = \int_0^t f(t')dt'$ and the angle variable ϕ is assumed to be constant over each pulse. A spin-1/2 particle interacting with an external magnetic field in the xy plane or a polarized photon moving through a half-wave plate, where the direction of the optical axis is given by ϕ, are possible realizations of $H^{(\mathrm{a})}$. Turning on $f(t)$ at $t = 0$, the system is described by the time evolution operator ($\hbar = 1$ from now on)

$$\begin{aligned}\mathcal{U}^{(\mathrm{a})}(t,0) &= e^{-i\int_0^t H^{(\mathrm{a})}(t')dt'} \\ &= \begin{pmatrix} \cos(\alpha_t/2) & -ie^{-i\phi}\sin(\alpha_t/2) \\ -ie^{i\phi}\sin(\alpha_t/2) & \cos(\alpha_t/2) \end{pmatrix}\end{aligned} \tag{2}$$

expressed in the computational qubit basis $\{|0\rangle,|1\rangle\}$, where $\sigma_z|n\rangle = (1-2n)|n\rangle$, $n = 0,1$. Here, $|0\rangle$ and $|1\rangle$ represent the north and south poles, respectively, of the Bloch sphere.

Suppose first that the system is prepared at one of the poles $|n\rangle$, $n = 0,1$, of the Bloch sphere. Turn on $f(t)$ and ϕ_1 for the time interval $[0,\tau]$; then switch to $-f(t-\tau)$ and ϕ_2 for the time interval $[\tau,2\tau]$. We choose $\alpha_\tau = \int_0^\tau f(t')dt' = \pi$. This evolves the system from the starting pole to the opposite pole along the semi-great-circle on the Bloch sphere corresponding to the fixed angle $\phi_1 - (-1)^n\frac{\pi}{2}$ and then back to the initial pole along a different semi-great-circle corresponding to the fixed angle $\phi_2 - (-1)^n\frac{\pi}{2}$. In other words, this evolution takes the system around the orange-slice-shaped path on the Bloch

*vahid.mousolou@lnu.se
†erik.sjoqvist@kemi.uu.se

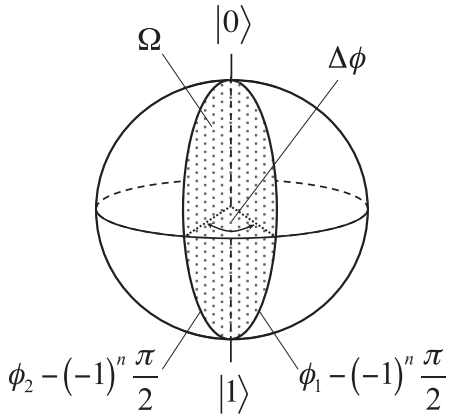

FIG. 1. Orange-slice-shaped path traced out by a qubit as it precesses around the Bloch sphere from one of the poles $|n\rangle, n = 0,1$, on a semi-great-circle to the opposite pole, and then returns on a different semi-great-circle to the initial pole. The GP is proportional to the solid angle $\Omega = 2(\phi_2 - \phi_1)$ enclosed by the orange-slice-shaped path.

sphere characterized by pairs of azimuthal angles $\phi_1 - (-1)^n \frac{\pi}{2}$ and $\phi_2 - (-1)^n \frac{\pi}{2}$ depending on the initial state $|n\rangle$ of the qubit, as sketched in Fig. 1. The final time evolution operator is given by

$$\begin{aligned}\mathcal{U}^{(\mathrm{a})}(2\tau,0) &= \mathcal{U}^{(\mathrm{a})}(2\tau,\tau;\phi_2)\mathcal{U}^{(\mathrm{a})}(\tau,0;\phi_1)\\ &= \begin{pmatrix} 0 & ie^{-i\phi_2} \\ ie^{i\phi_2} & 0 \end{pmatrix}\begin{pmatrix} 0 & -ie^{-i\phi_1} \\ -ie^{i\phi_1} & 0 \end{pmatrix}\\ &= \begin{pmatrix} e^{-i\Omega/2} & 0 \\ 0 & e^{i\Omega/2} \end{pmatrix}, \end{aligned} \tag{3}$$

where $\Omega = 2(\phi_2 - \phi_1) = 2\Delta\phi$ is the solid angle subtended by the two semi-great-circles. The dynamical phases $-\int_0^t \langle n|H^{(\mathrm{a})}(t')|n\rangle dt'$, $n = 0,1$, vanish along this evolution, and hence the accumulated phases are purely geometric, defining the geometric phase-shift gate

$$|n\rangle \mapsto e^{-i(1/2-n)\Omega}|n\rangle, \quad n = 0,1. \tag{4}$$

The GP associated with this orange-slice-shaped path has been measured in several experiments [10–14].

III. NON-ABELIAN GENERALIZATION

A. Model system

We now extend the above Abelian setting to the non-Abelian case. Note that while the Abelian GP appears in the evolution of a pure state, which constitutes a one-dimensional subspace of the full Hilbert space, the non-Abelian GP is a property of a higher-dimensional subspace [4,5]. Thus, we need more than a single qubit to achieve this. The general structure that we have in mind is described by a cyclic chain of four qubits with nearest-neighbor interaction described by the Hamiltonian

$$H = \frac{1}{2}F(t)\sum_{k=1}^{4}\left(J_{k,k+1}R^{XY}_{k,k+1} + D^{z}_{k,k+1}R^{\mathrm{DM}}_{k,k+1}\right), \tag{5}$$

where $R^{XY}_{k,k+1} = \frac{1}{2}(\sigma_x^k\sigma_x^{k+1} + \sigma_y^k\sigma_y^{k+1})$ and $R^{\mathrm{DM}}_{k,k+1} = \frac{1}{2}(\sigma_x^k\sigma_y^{k+1} - \sigma_y^k\sigma_x^{k+1})$ are XY and Dzyalochinski-Moriya (DM) terms with coupling strengths $J_{k,k+1}$ and $D^z_{k,k+1}$, respectively. $F(t)$ turns on and off all qubit interactions simultaneously. The cyclic nature of the qubit chain is reflected in the boundary conditions $J_{4,5}R^{XY}_{4,5} = J_{4,1}R^{XY}_{4,1}$ and $D^z_{4,5}R^{\mathrm{DM}}_{4,5} = D^z_{4,1}R^{\mathrm{DM}}_{4,1}$.

The Hamiltonian in Eq. (5) preserves the single-excitation subspace $\mathcal{H}_{\mathrm{eff}}$ of the four qubits spanned by the following ordered basis:

$$\mathcal{B} = \{|1000\rangle, |0010\rangle, |0100\rangle, |0001\rangle\}, \tag{6}$$

where $|1000\rangle$, say, stands for $|1\rangle_1|0\rangle_2|0\rangle_3|0\rangle_4$, $|0\rangle_k$ ($|1\rangle_k$) being the eigenvector of the z component of the Pauli operator σ_z^k at site k corresponding to the eigenvalue 1 (-1). In the basis $\mathcal{B}$, the Hamiltonian takes the form

$$H^{(\mathrm{na})} = \frac{1}{2}F(t)\begin{pmatrix} 0 & T \\ T^\dagger & 0 \end{pmatrix}, \tag{7}$$

where

$$T = \begin{pmatrix} J_{12} - iD^z_{12} & J_{41} + iD^z_{41} \\ J_{23} + iD^z_{23} & J_{34} - iD^z_{34} \end{pmatrix} = USV^\dagger. \tag{8}$$

Here, U, V, and S are the unitary and diagonal positive parts in the singular-value decomposition of T. For simplicity, we assume $S > 0$.

There are different physical realizations of the Hamiltonian in Eq. (7). First, it describes the single-excitation subspace of a cyclic chain of four coupled quantum dots with double occupancy of each dot being prevented by strong Hubbard-repulsion terms [18]. Secondly, $H^{(\mathrm{na})}$ is relevant to a square optical lattice of two-level atoms with synthetic spin-orbit coupling localized at each lattice site allowing for the desired combination of XY and DM interactions, by suitable parameter choices [19]. Finally, the Ruderman-Kittel-Kasuya-Yosida interaction in three-dimensional topological insulators may be used to obtain the XY and DM interaction terms in $H^{(\mathrm{na})}$ [20].

The Hamiltonian in Eq. (7) splits the effective state space $\mathcal{H}_{\mathrm{eff}}$ into two orthogonal subspaces, i.e.,

$$\mathcal{H}_{\mathrm{eff}} = M_0 \oplus M_1, \tag{9}$$

where $M_0 = \mathrm{Span}\{|1000\rangle, |0010\rangle\}$ and $M_1 = \mathrm{Span}\{|0100\rangle, |0001\rangle\}$. This implies that in the basis $\mathcal{B}$ the time evolution operator splits into 2×2 blocks according to [18]

$$\mathcal{U}^{(\mathrm{na})}(t,0) = \begin{pmatrix} U\cos(\alpha_t S/2)\,U^\dagger & -iU\sin(\alpha_t S/2)\,V^\dagger \\ -iV\sin(\alpha_t S/2)\,U^\dagger & V\cos(\alpha_t S/2)\,V^\dagger \end{pmatrix}, \tag{10}$$

where $\alpha_t = \int_0^t F(t')dt'$.

The non-Abelian orange-slice-shaped path is realized by first applying a pulse over $[0,\tau]$ with $F(t)$ and $T_1 = U_1S_1V_1^\dagger$, followed by a pulse over $[\tau',\tau'+\tau'']$ with $-\tilde{F}(t-\tau')$ and $T_2 = U_2S_2V_2^\dagger$. We assume that $\tau'+\tau'' > \tau' > \tau$ and that the Hamiltonian is completely turned off on $[\tau,\tau']$. Note that the size of the time gap $\tau' - \tau$ is restricted only by errors, such as parameter noise and decoherence, and can therefore be arbitrarily long in the ideal error-free case. By choosing parameters such that $\cos(\alpha_\tau S_1/2) = \cos(\tilde{\alpha}_{\tau''}S_2/2) =$

0, $\sin(\alpha_\tau S_1/2) = Z^{p_1}$, and $\sin(\tilde{\alpha}_{\tau''} S_2/2) = Z^{p_2}$, where $\tilde{\alpha}_t = \int_0^t \tilde{F}(t')dt'$, $p_1, p_2 = 0,1$, and $Z = \mathrm{diag}\{1, -1\}$, we obtain the final time evolution operator

$$\begin{aligned}
&\mathcal{U}^{(\mathrm{na})}(\tau+\tau'',0)\\
&\quad = \mathcal{U}^{(\mathrm{na})}(\tau'+\tau'',\tau';T_2)\mathcal{U}^{(\mathrm{na})}(\tau,0;T_1)\\
&\quad = \begin{pmatrix} 0 & iU_2 Z^{p_2} V_2^\dagger \\ iV_2 Z^{p_2} U_2^\dagger & 0 \end{pmatrix}\\
&\qquad \times \begin{pmatrix} 0 & -iU_1 Z^{p_1} V_1^\dagger \\ -iV_1 Z^{p_1} U_1^\dagger & 0 \end{pmatrix}\\
&\quad = \begin{pmatrix} U_2 Z^{p_2} V_2^\dagger V_1 Z^{p_1} U_1^\dagger & 0 \\ 0 & V_2 Z^{p_2} U_2^\dagger U_1 Z^{p_1} V_1^\dagger \end{pmatrix} \qquad (11)
\end{aligned}$$

expressed with respect to the basis $\mathcal{B}$.

By considering the evolution of the orthogonal subspaces M_0 and M_1 in each pulse, one may notice that the two unitaries $U(C_0) = U_2 Z^{p_2} V_2^\dagger V_1 Z^{p_1} U_1^\dagger$ and $U(C_1) = V_2 Z^{p_2} U_2^\dagger U_1 Z^{p_1} V_1^\dagger$ are purely geometric since the Hamiltonian $H^{(\mathrm{na})}$ vanishes on M_0 and M_1 separately [5]. In fact, for each $q = 0,1$, $U(C_q)$ is the nonadiabatic non-Abelian GP associated with the evolution of the subspace M_q along the orange-slice-shaped path C_q via the midpoint M_{1-q} back to itself, as depicted in Fig. 2. Thus, the time evolution operator $\mathcal{U}^{(\mathrm{na})}(\tau'+\tau'',0)$ is fully determined by the pair of closed paths C_0 and C_1 in the Grassmannian $\mathcal{G}(4;2)$, i.e., the space of two-dimensional subspaces of a four-dimensional Hilbert space [21].

In the following we will justify the orange-slice nature of the path C_q and propose a measurement mechanism of the associated non-Abelian GP $U(C_q)$.

B. Geometric interpretations

The path C_q is formed of two geodesic paths $\gamma_q^{(1)}$ and $\gamma_q^{(2)}$ in $\mathcal{G}(4;2)$. To see this, consider the Stiefel manifold $\mathcal{S}(4;2)$, which is the space of two-frames in the effective four-dimensional Hilbert space $\mathcal{H}_{\mathrm{eff}}$. There is a natural projection

$$\Pi \ : \ \mathcal{S}(4;2) \longrightarrow \mathcal{G}(4;2), \qquad (12)$$

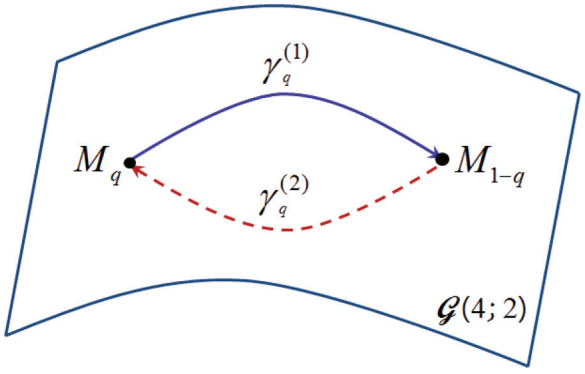

FIG. 2. (Color online) Schematic picture of orange-slice-shaped paths $C_q = \gamma_q^{(1)} * \gamma_q^{(2)}$, $q = 0,1$, in the Grassmannian $\mathcal{G}(4;2)$. $\gamma_q^{(1)}$ and $\gamma_q^{(2)}$ are the two geodesic edges of the orange-slice-shaped path C_q, which connect the two orthogonal poles M_0 and M_1 in $\mathcal{G}(4;2)$.

which takes each frame to the corresponding subspace spanned by that frame. For each $q = 0,1$ and $l = 1,2$ we may introduce the new orthonormal basis vectors of $\mathcal{H}_{\mathrm{eff}}$ as

$$\begin{aligned}
\left|e_1^{(l,q)}\right\rangle &= \Lambda(q)|(1-q)q00\rangle,\\
\left|e_2^{(l,q)}\right\rangle &= \Lambda(q)|00(1-q)q\rangle,\\
\left|e_3^{(l,q)}\right\rangle &= (-1)^l\Lambda(q)|q(1-q)00\rangle,\\
\left|e_4^{(l,q)}\right\rangle &= (-1)^l\Lambda(q)|00q(1-q)\rangle,
\end{aligned} \qquad (13)$$

where the unitary operator $\Lambda(q)$ has the form

$$\Lambda(q) = \begin{pmatrix} i^q U & 0 \\ 0 & i^{1-q} V \end{pmatrix} \qquad (14)$$

in the basis $\mathcal{B}$. With the above notations, one may notice that $\Pi[|e_1^{(l,q)}\rangle, |e_2^{(l,q)}\rangle] = M_q$ and $\Pi[|e_3^{(l,q)}\rangle, |e_4^{(l,q)}\rangle] = M_{1-q}$.

In the non-Abelian case, subspaces M_0 and M_1 play the same role as the two opposite poles in the Abelian case. The non-Abelian evolution takes the system initially prepared in the subspace M_q to its orthogonal complement M_{1-q} along the geodesic:

$$\begin{aligned}
&\gamma_q^{(1)} \ : \ [0,\tau] \ni t\\
&\quad \longrightarrow \Pi\Big[\cos\left(\frac{\alpha_t}{2}s_{1;1}\right)\left|e_1^{(1,q)}\right\rangle + \sin\left(\frac{\alpha_t}{2}s_{1;1}\right)\left|e_3^{(1,q)}\right\rangle,\\
&\qquad \cos\left(\frac{\alpha_t}{2}s_{1;2}\right)\left|e_2^{(1,q)}\right\rangle + \sin\left(\frac{\alpha_t}{2}s_{1;2}\right)\left|e_4^{(1,q)}\right\rangle\Big] \qquad (15)
\end{aligned}$$

in $\mathcal{G}(4;2)$, where $S_1 = \mathrm{diag}\{s_{1;1}, s_{1;2}\} > 0$ [22]. This is followed by evolving the subspace M_{1-q} back to the initial subspace M_q along a different geodesic in $\mathcal{G}(4;2)$ given by

$$\begin{aligned}
&\gamma_q^{(2)} \ : \ [\tau',\tau'+\tau''] \ni t\\
&\quad \longrightarrow \Pi\Big[\cos\left(\frac{\tilde{\alpha}_t}{2}s_{2;1}\right)\left|e_1^{(2,1-q)}\right\rangle + \sin\left(\frac{\tilde{\alpha}_t}{2}s_{2;1}\right)\left|e_3^{(2,1-q)}\right\rangle,\\
&\qquad \cos\left(\frac{\tilde{\alpha}_t}{2}s_{2;2}\right)\left|e_2^{(2,1-q)}\right\rangle + \sin\left(\frac{\tilde{\alpha}_t}{2}s_{2;2}\right)\left|e_4^{(2,1-q)}\right\rangle\Big], \qquad (16)
\end{aligned}$$

where $S_2 = \mathrm{diag}\{s_{2;1}, s_{2;2}\} > 0$. In fact for each $q = 0,1$, the geodesics γ_q^l, $l = 1,2$, form the two edges of the orange-slice-shaped path C_q, which connect the two orthogonal subspaces M_0 and M_1 in $\mathcal{G}(4;2)$.

The orange-slice nature of the path C_q in $\mathcal{G}(4;2)$ and the resulting non-Abelian GP may be more transparent in the following intuitive picture. We first examine the corresponding paths leading to the Abelian GPs in Eq. (3). Let us consider the initial state $|0\rangle$, which evolves as

$$\begin{aligned}
|0\rangle &\mapsto \mathcal{U}^{(\mathrm{a})}(t,0)|0\rangle\\
&= |\psi_0(t)\rangle = \cos(\alpha_t/2)|0\rangle - ie^{i\phi}\sin(\alpha_t/2)|1\rangle. \qquad (17)
\end{aligned}$$

This vector rotates at the same constant angle around the fixed vectors

$$|\pm(\phi)\rangle = \frac{1}{\sqrt{2}}(|0\rangle \pm e^{i\phi}|1\rangle) \qquad (18)$$

in the sense that the fidelity is time independent, viz., $|\langle\pm(\phi)|\psi_0(t)\rangle| = \frac{1}{\sqrt{2}}$. Thus, $|\psi_0(t)\rangle$ is mutually unbiased with

respect to each of $|\pm(\phi)\rangle$. The vectors $|\pm(\phi)\rangle$ are eigenvectors of the fixed Pauli operator $\mathbf{n}\cdot\boldsymbol{\sigma} = \cos(\phi)\sigma_x + \sin(\phi)\sigma_y$, $\mathbf{n}$ being the rotation axis of the Bloch vector for each semi-great-circle and $\boldsymbol{\sigma} = (\sigma_x,\sigma_y,\sigma_z)$.

The above picture translates to the non-Abelian setting as follows. We consider the evolution of M_0 in $\mathcal{G}(4;2)$. This evolution can be viewed as a rotating complex two-plane in the four-dimensional complex vector space $\mathcal{H}_{\text{eff}}$. This plane is spanned by the frame $\{\mathcal{U}^{(\text{na})}(t,0)|\mu_1\rangle,\mathcal{U}^{(\text{na})}(t,0)|\mu_2\rangle\}$, where $|\mu_1\rangle$ and $|\mu_2\rangle$ can be any pair of orthonormal vectors spanning M_0. In particular, the vectors $|\mu_1\rangle = \Lambda(0)|1000\rangle$ and $|\mu_2\rangle = \Lambda(0)|0010\rangle$ define the two-frame

$$|\mu_1(t)\rangle = \Lambda(0)\left[\cos\left(\frac{\alpha_t}{2}s_1\right)|1000\rangle - \sin\left(\frac{\alpha_t}{2}s_1\right)|0100\rangle\right],$$
$$|\mu_2(t)\rangle = \Lambda(0)\left[\cos\left(\frac{\alpha_t}{2}s_2\right)|0010\rangle - \sin\left(\frac{\alpha_t}{2}s_2\right)|0001\rangle\right], \tag{19}$$

where $S = \text{diag}\{s_1,s_2\} > 0$. Thus, $P(t) = |\mu_1(t)\rangle\langle\mu_1(t)| + |\mu_2(t)\rangle\langle\mu_2(t)|$ projects onto the rotating complex two-plane $M(t)$.

Now, there are fixed two-dimensional subspaces $M_\pm$ with corresponding projection operators $P_\pm$ that satisfy the fidelity relations

$$\text{Tr}[P_\pm P(t)] = 1, \tag{20}$$

being again the same for $\pm$ and independent of time. Explicitly, a two-frame spanning $M_\pm$ is

$$|\psi_\pm\rangle = \frac{1}{\sqrt{2}}\Lambda(0)(|1000\rangle \pm i|0100\rangle),$$
$$|\psi_\pm^\perp\rangle = \frac{1}{\sqrt{2}}\Lambda(0)(|0010\rangle \pm i|0001\rangle), \tag{21}$$

which can be used to prove that the two subspaces $M(t)$ and $M_\pm$ are mutually unbiased. Similar scenarios hold for evolutions initiated at $|1\rangle$ and M_1. Thus, in analogy with the above Abelian case, we may understand the orange-slice nature of C_q as a rotation of the complex two-plane around some fixed subspaces.

Notice that $U_l Z^{p_l} V_l^\dagger$ is a U(2) transformation and therefore can be put in the form $e^{-i\chi_l}e^{-i\varphi_l\mathbf{n}_l\cdot\mathbf{X}/2}$, where χ_l and φ_l are real valued, $\mathbf{n}_l$ is a real unit vector, and $\mathbf{X}$ is the vector of standard Pauli matrices acting on M_0 or M_1. Thus, the GPs may be written

$$U(C_0) = e^{-i\Delta\chi}e^{-i\varphi_2\mathbf{n}_2\cdot\mathbf{X}/2}e^{i\varphi_1\mathbf{n}_1\cdot\mathbf{X}/2},$$
$$U(C_1) = e^{i\Delta\chi}e^{i\varphi_2\mathbf{n}_2\cdot\mathbf{X}/2}e^{-i\varphi_1\mathbf{n}_1\cdot\mathbf{X}/2}, \tag{22}$$

where $\Delta\chi = \chi_2 - \chi_1$.

The non-Abelian contributions $e^{-i\varphi_2\mathbf{n}_2\cdot\mathbf{X}/2}e^{i\varphi_1\mathbf{n}_1\cdot\mathbf{X}/2}$ and $e^{i\varphi_2\mathbf{n}_2\cdot\mathbf{X}/2}e^{-i\varphi_1\mathbf{n}_1\cdot\mathbf{X}/2}$ represent twists caused by the nontrivial geometry of $\mathcal{G}(4;2)$. The non-Abelian nature is apparent from the fact that the two factors in each GP do not commute when $\mathbf{n}_2 \neq \mathbf{n}_1$. The unitary action on M_q that is induced by C_q is universal since the SU(2) parameters φ_1, φ_2, $\mathbf{n}_1$, and $\mathbf{n}_2$ can in principle be chosen independently. Thus, this unitary action serves as a universal gate on a single qubit encoded in M_q. On the other hand, the Abelian parts $e^{\pm i\Delta\chi}$ are global phases and therefore unimportant for such single-qubit gate operations.

C. Meaurement scheme

The non-Abelian GPs $U(C_q)$ can be measured by applying unitary operators W_q acting on the subspaces M_q immediately after the realization of the orange-slice-shaped path. This results in the unitary transformation $W_0U(C_0)\oplus W_1U(C_1)$. For an input state $|\psi\rangle \in \mathcal{H}_{\text{eff}}$, the survival probability reads

$$p = |\langle\psi|W_0U(C_0)\oplus W_1U(C_1)|\psi\rangle|^2 \leqslant 1 \tag{23}$$

with equality for all $|\psi\rangle$ when $W_0^\dagger \oplus W_1^\dagger = U(C_0)\oplus U(C_1)$ up to an overall U(1) phase factor. In this way, the non-Abelian SU(2) part of $U(C_q)$ can be measured by varying W_q until the maximum is reached.

We now describe how this scheme can be implemented in a cyclic chain of four coupled quantum dots at half filling [18,23]. Appropriate XY and DM terms can be designed in this system by utilizing the interplay between electron-electron repulsion and spin-orbit interaction. In this way, $U(C_q)$ and W_q can be realized in the invariant four-dimensional subspace, our $\mathcal{H}_{\text{eff}}$, spanned by the local single-spin-flip states $|\downarrow\uparrow\uparrow\uparrow\rangle,\ldots,|\uparrow\uparrow\uparrow\downarrow\rangle$ of the electrons.

The non-Abelian GPs $U(C_q)$ are realized in $\mathcal{H}_{\text{eff}}$ by turning on and off appropriate nearest-neighbor interactions, which results in an effective Hamiltonian of the form given by Eq. (7). The variable unitary operators W_q should be 2×2 diagonal blocks in $\mathcal{H}_{\text{eff}}$, which is achieved by turning on and off the next-nearest-neighbor interactions as described by the Hamiltonan

$$h = f(s)\left[\sum_{k=1}^{2}\left(J_{k,k+2}R_{k,k+2}^{XY} + D_{k,k+2}^{z}R_{k,k+2}^{\text{DM}}\right) + E(Z_1+Z_2)\right]. \tag{24}$$

To realize full variability in W_q, we have added the term $E(Z_1+Z_2)$ with $Z_1 = |\downarrow\uparrow\uparrow\uparrow\rangle\langle\downarrow\uparrow\uparrow\uparrow| - |\uparrow\uparrow\downarrow\uparrow\rangle\langle\uparrow\uparrow\downarrow\uparrow|$ and $Z_2 = |\uparrow\downarrow\uparrow\uparrow\rangle\langle\uparrow\downarrow\uparrow\uparrow| - |\uparrow\uparrow\uparrow\downarrow\rangle\langle\uparrow\uparrow\uparrow\downarrow|$, corresponding to a local energy shift of the first and second sites relative to the third and fourth sites (obtained, for instance, by applying an inhomogeneous magnetic field over the four-dot system). In the ordered basis $\mathcal{B} = \{|\downarrow\uparrow\uparrow\uparrow\rangle,|\uparrow\downarrow\uparrow\uparrow\rangle,|\uparrow\downarrow\uparrow\uparrow\rangle,|\uparrow\uparrow\uparrow\downarrow\rangle\}$ of the single-spin-flip-subspace, $h = f(s)T_0\oplus T_1$ with the 2×2 blocks

$$T_0 = \begin{pmatrix} E & J_{13} + iD_{13}^z \\ J_{13} - iD_{13}^z & -E \end{pmatrix},$$
$$T_1 = \begin{pmatrix} E & J_{24} + iD_{24}^z \\ J_{24} - iD_{24}^z & -E \end{pmatrix}. \tag{25}$$

The variable unitary $W_0\oplus W_1$ is generated by h and takes the desired block-diagonal form $W_0\oplus W_1 = e^{-ib_tT_0}\oplus e^{-ib_tT_1}$ with $b_t = \int_0^t f(s)ds$ the pulse area. Thus, $e^{-ib_tT_0}$ and $e^{-ib_tT_1}$ are SU(2) operators that can be fully varied by changing the parameters $J_{k,k+1}, D_{k,k+1}$, and E.

To measure the non-Abelian GPs, prepare first an appropriate initial state in the four-dot system by polarizing the spins along the z direction by an external magnetic field followed by a single spin flip induced by a local magnetic field in the x direction at one of the sites [24]. Suppose we apply the spin flip

to the first site, leading to the initial spin state $|\psi\rangle = |\downarrow\uparrow\uparrow\uparrow\rangle \in \mathcal{H}_{\text{eff}}$ of the four electrons. In this way, a measurement of $U(C_0)$ can be performed by implementing sequentially $\mathcal{U}^{(\text{na})}(\tau,0;T_1)$, $\mathcal{U}^{(\text{na})}(\tau'+\tau'',\tau';T_2)$, and $e^{-ib_t h}$. $U(C_0)$ can be measured by varying the parameters J_{13}, D_{13}, E, and b_t until the probability $p = |\langle\downarrow\uparrow\uparrow\uparrow|e^{-ib_t T_0}U(C_0)|\downarrow\uparrow\uparrow\uparrow\rangle|^2$ reaches its maximum at $e^{ib_t T_0} = U(C_0)$.

IV. CONCLUSIONS

We have developed a non-Abelian generalization of the concept of orange-slice-shaped paths to allow for direct measurement of the non-Abelian GP in nonadiabatic evolution. The geometric interpretation of this non-Abelian GP is quite different from that in terms of the solid angle enclosed on the Bloch sphere of its Abelian counterpart. Instead, the orange-slice nature of the path underlying the non-Abelian GP is associated with pairs of geodesics in the Grassmannian manifold $\mathcal{G}(4;2)$, i.e., the space of two-dimensional subspaces of the system's effective four-dimensional Hilbert space.

The proposed method for measuring the non-Abelian GP can be implemented in a cyclic chain of four qubits that can be realized in different physical settings, such as in quantum-dot, optical-lattice, and topological-insulator architectures. The realizations and their readout require interactions that can simultaneously be turned on and off in a controlled way.

The present work suggests an alternative way to reach closed paths in the Grassmannian $\mathcal{G}(4;2)$, which are the main ingredient in achieving universal holonomic quantum gates proposed in [18] to perform fault-tolerant quantum information processing. The orange-slice-shaped loops considered here are encouraged by a common experimental method for measuring the Abelian GP [10–14]. This certain type of closed path is substantially different from those considered in Ref. [18] in that the orange-slice-shaped loops are accomplished by applying sequentially two different pulses while the loops in Ref. [18] are the results of single pulses. Moreover, the orange-slice technique allows for arbitrary SU(2) holonomic transformations in a single-loop scenario, while the scheme in Ref. [18] can achieve this only by combining at least two loops.

It is important that different approaches and schemes for holonomic quantum computation be thoroughly explored and compared with one another. This would help to optimize a setup with respect to robustness and, at the same time, to make it accessible experimentally and amenable to external manipulation. Such a setup would be essential to construct scalable, compact, and reproducible building blocks of quantum computers. This would also further improve our understanding of the relation between abstract theoretical objects, such as the geometry of the Grassmannian manifolds, and practically observed quantum phenomena.

ACKNOWLEDGMENTS

V.A.M. is supported by the Department of Physics and Electrical Engineering at Linnaeus University (Sweden) and by the National Research Foundation (VR). E.S. acknowledges support from the National Research Foundation and the Ministry of Education (Singapore).

[1] M. V. Berry, Proc. R. Soc. London, Ser. A **329**, 45 (1984).
[2] Y. Aharonov and J. S. Anandan, Phys. Rev. Lett. **58**, 1593 (1987).
[3] J. Samuel and R. Bhandari, Phys. Rev. Lett. **60**, 2339 (1988).
[4] F. Wilczek and A. Zee, Phys. Rev. Lett. **52**, 2111 (1984).
[5] J. Anandan, Phys. Lett. A **133**, 171 (1988).
[6] E. Sjöqvist, A. K. Pati, A. Ekert, J. S. Anandan, M. Ericsson, D. K. L. Oi, and V. Vedral, Phys. Rev. Lett. **85**, 2845 (2000).
[7] D. M. Tong, E. Sjöqvist, L. C. Kwek, and C. H. Oh, Phys. Rev. Lett. **93**, 080405 (2004).
[8] A. Bohm, A. Mostafazadeh, H. Koizumi, Q. Niu, and J. Zwanziger, *The Geometric Phase in Quantum Systems* (Springer, New York, 2003).
[9] D. Chruściński and A. Jamiołkowski, *Geometric Phases in Classical and Quantum Mechanics*, (Springer Science+Business Media, New York, 2004).
[10] P. G. Kwiat and R. Y. Chiao, Phys. Rev. Lett. **66**, 588 (1991).
[11] B. E. Allman, H. Kaiser, S. A. Werner, A. G. Wagh, V. C. Rakhecha, and J. Summhammer, Phys. Rev. A **56**, 4420 (1997).
[12] J. Du, P. Zou, M. Shi, L. C. Kwek, J.-W. Pan, C. H. Oh, A. Ekert, D. K. L. Oi, and M. Ericsson, Phys. Rev. Lett. **91**, 100403 (2003).
[13] L. Rippe, B. Julsgaard, A. Walther, Yan Ying, and S. Kröll, Phys. Rev. A **77**, 022307 (2008).
[14] S. Sponar, J. Klepp, R. Loidl, S. Filipp, K. Durstberger-Rennhofer, R. A. Bertlmann, G. Badurek, H. Rauch, and Y. Hasegawa, Phys. Rev. A **81**, 042113 (2010).
[15] E. Sjöqvist, D. M. Tong, B. Hessmo, L. M. Andersson, M. Johansson, and K. Singh, New J. Phys. **14**, 103035 (2012).
[16] A. A. Abdumalikov, J. M. Fink, K. Juliusson, M. Pechal, S. Berger, A. Wallraff, and S. Filipp, Nature (London) **496**, 482 (2013).
[17] G. Feng, G. Xu, and G. Long, Phys. Rev. Lett. **110**, 190501 (2013).
[18] V. A. Mousolou, C. M. Canali, and E. Sjöqvist, New J. Phys. **16**, 013029 (2014).
[19] J. Radić, A. Di Ciolo, K. Sun, and V. Galitski, Phys. Rev. Lett. **109**, 085303 (2012).
[20] J.-J. Zhu, D.-X. Yao, S.-C. Zhang, and K. Chang, Phys. Rev. Lett. **106**, 097201 (2011).
[21] I. Bengtsson and K. Życzkowski, *Geometry of Quantum States* (Cambridge University Press, Cambridge, 2006), Chap. 4.9.
[22] For geodesics in Grassmann manifolds, see J. Zhou, Soochow J. Math. **24**, 329 (1998).
[23] V. A. Mousolou, C. M. Canali, and E. Sjöqvist, Europhys. Lett. **103**, 60011 (2013).
[24] M. S. Grinolds, P. Maletinsky, S. Hong, M. D. Lukin, R. L. Walsworth, and A. Yacoby, Nat. Phys. **7**, 687 (2011).